Thus, we had $n \sim 200$ points per run, with equal or unequal spacing (depending on the observing method) and some gaps attributable to calibration and optical depth measurements. The data for each run were then analysed by the Fourier technique of Deeming[11]. Because of the noise and data spacing, many peaks are apparent on the spectrum of a typical run. Among these peaks, one corresponding to a 15.7-min period is clearly visible on many nights and is shown in Fig. 1*a* for the run on 24 April 1981.

For a closer inspection of the observations, we have used the periodogram technique of Warner and Robinson[12], which is better suited for noisy data and non-sinusoidal variations. On nights where Fourier analysis indicates the presence of a clear 15.7-min variation, the periodogram technique helps to confirm the period, as well as giving the phase and the light curve of the variations.

On several occasions we were able to observe OJ287 on several consecutive nights. Although the long gaps between runs cause strong aliasing peaks, these can be identified by calculating the spectral window. If the 15.7-min variation is real, we would expect it to stand out more clearly in the combined data, whereas spurious peaks due to noise, unable to keep either phase or period from night to night, would be suppressed. Figure 1*b* shows the results of Fourier analysis for the combined runs of 5–7 March 1982 (595 observing points). Periodogram analysis gives a period of 943 s, in accordance with Fourier analysis. A comparison with similar data from combined runs, May 1981 onwards, indicates that the period may be constant to an accuracy of 1 s yr^{-1}.

To identify possible instrumental variations, we have made similar observations of a number of other sources and pure background noise, analysing these using the same techniques. Certain periodicities, for example, the peaks marked C in Fig. 1*b*, are caused by the radome and the variations in the electric current and are identified in most observing runs. Although no observing run is ever exactly repeatable and the periodicity could perhaps have been caused by some unknown mechanism, the most probable explanation is that the 15.7-min periodicity is intrinsic to OJ287, as we have not detected it in any of the other sources.

To ascertain whether the periodicity would be detectable with other instruments, simultaneous measurements were made on 26 February 1982 using the radio telescope at Metsähovi operating on 22 GHz, a double-beam chopping photometer using the 60-cm telescope of Metsähovi Observatory and using a similar photometer coupled to the 60-cm telescope at Turku Observatory, about 150 km west of Metsähovi. (The construction and operating principle of the photometers have been described by Piirola[13].) A standard observing procedure, with comparison stars measured at regular intervals, was followed. The measurements were made through the B filter. At the time of the observations, OJ287 was rather faint, with B (magnitude) = 14.6 mag, and the noise level of optical observations was rather high. The power spectra of all three runs were calculated and compared with each other and all three instruments showed a peak near the 15.7-min period: the radio telescope at 945 ± 15 s, the Metsähovi photometer at 980 ± 35 s and the Turku photometer at 935 ± 35 s, with the formal error limits derived from half-widths of the peaks.

To check for a coincidence, we further investigated all the peaks visible in each spectrum using the periodogram technique. In the case of the optical observations, the only periodicities found to have the same phase (within observational error) were those corresponding to the 15.7-min peak. In addition, the radio observations gave a similar light curve, but out-of-phase, and the amplitude of the variations seems to be the same at both wavelengths.

OJ287 was again observed with the 140-ft telescope of the National Radio Astronomy Observatory (NRAO) on 23 May 1983. The effective single integration times were 27 s and the total integration lasted 7.6 h, producing 330 observing points in all. Figure 2 shows the resulting power spectrum and Fig. 3 gives the mean light curve of the 15.7-min variation together with 2σ error bars. In addition to the 15.7-min power spectrum peak, strong peaks are visible at 33 min and 13 min. Both the 15.7-min peak and the 13.0-min peak were outstanding in the Metsähovi 37-GHz data (298 points over 6 h), also taken on 23 May 1983, but the 33-min peak was not observed.

Consequently, the 13-min periodic component, which has appeared on several occasions, has also attracted our attention. In addition, others[14] have observed a strong periodicity at 23 min between January and March 1983 in OJ287. Whether these periods are as durable as the 15.7-min period remains to be seen. Even in the case of the 15.7-min period, there are strong fluctuations in the amplitude, of $>15\%$ to $\sim 1\%$. An interesting parallel may be provided by the infrared observations of Wolstencroft *et al.*[2], where rapid, but presumably nonperiodic, variability was seen on only one night out of a total of 12, accompanied by a change in the shape of the infrared continuum. Simultaneous observations with different instruments are the only way to obtain definite proof for the existence of variations of this kind.

If only a single periodic component is confirmed, one may identify it with the rotation period of a single supermassive body[15–17]. However, if the evidence for many periodic components is sustained, then it is more probable that we are observing keplerian motion around a single dominant body with many different orbital radii, analogous to the modulation of the radio emission of Jupiter by its innermost moons. In any case, short periods such as 15.7 min indicate a relatively small mass for the central body ($\lesssim 10^7 M_\odot$) and a problem with the high luminosity of the quasar[4,5].

The work has been supported by a grant from the Academy of Finland. We thank the NRAO for the allocation of observing time for their 140-ft telescope and S. Haarala for help with the observations and data analysis. NRAO is operated by Associated Universities, Inc., under contract with the NSF.

Received 6 November 1984; accepted 15 January 1985.

1. Efanov, V. A., Moiseev, I. G., Nesterov, N. S. & Wright, A. *Bull. Crimean astrophys. Obs.* **61**, 58–62 (1980).
2. Wolstencroft, R. D., Gilmore, G. & Williams, P. M. *Mon. Not. R. astr. Soc.* **201**, 479–485 (1982).
3. Kulshrestha, A. K., Joshi, U. C. & Deshpande, M. R. *Nature* **311**, 733–734 (1984).
4. Elliot, J. L. & Shapiro, S. L. *Astrophys. J.* **192**, L3–L6 (1974).
5. Abramowicz, M. A. & Nobili, L. *Nature* **300**, 506–508 (1982).
6. Visvanathan, N. & Elliot, J. L. *Astrophys. J.* **179**, 721–730 (1973).
7. Frohlich, A., Goldsmith, S. & Weistrop, D. *Mon. Not. R. astr. Soc.* **168**, 417–425 (1974).
8. Kiplinger, A. J. *Astrophys. J.* **191**, L109–L110 (1974).
9. Salonen, S. *et al. Astr. Astrophys. Suppl.* **51**, 47–62 (1983).
10. Lehto, H. *et al. Turku University Observatory Informo* No. 52 (1981).
11. Deeming, T. J. *Astrophys. Space Sci.* **36**, 137–158 (1974).
12. Warner, B. & Robinson, E. L. *Mon. Not. R. astr. Soc.* **159**, 101–111 (1972).
13. Piirola, V. *Ann. Acad. Sci. fennicae* A VI, No. 418 (1975).
14. Carrasco, L., Dultzin-Hacyan, D. & Cruz-Gonzalez, I. *Nature* **314**, 146–148 (1985).
15. Morrison, P. *Astrophys. J.* **157**, L73–L76 (1969).
16. Woltjer, L. *Pont. Acad. Sci. Scripta Varia* **35**, 477–483 (1971).
17. Morrison, P. & Cavaliere, A. *Pont. Acad. Sci. Scripta Varia* **35**, 485–509 (1971).

Influences of precipitation changes and direct CO_2 effects on streamflow

T. M. L. Wigley & P. D. Jones

Climatic Research Unit, School of Environmental Sciences, University of East Anglia, Norwich NR4 7TJ, UK

Increasing atmospheric carbon dioxide concentrations are expected[1] to cause major changes in the world's climate over the next 50–100 yr. The impact of such changes on water resources, through changing precipitation and evaporation, will, however, be complicated by the direct effects of increasing CO_2 on vegetation. In controlled environment experiments, higher CO_2 levels cause the stomata of plants to close down, decreasing their rate of transpiration and increasing their water use efficiency[2]. Reduced evapotranspiration would make more water available as runoff and could

tend to offset the effects of any CO_2-induced reductions in precipitation or enhance the effects of precipitation increases. We consider here, in a simple but revealing analysis, the relative sensitivity of runoff to these two processes, changes in precipitation and changes in evapotranspiration. We show that, for low runoff ratios, small changes in precipitation may cause large changes in runoff. The magnitude and direction of these changes is, however, strongly dependent on the magnitude of the direct CO_2 effect on plant evapotranspiration.

Although much has been published on the climatic effects of increasing CO_2, few studies have considered the impact on water resources. Revelle and Waggoner[3] used empirical relationships to study the effect on water supplies in the western United States of a 10% reduction in precipitation and a 2 °C warming. They suggested that there could be large reductions in river flow. Rind and Lebedeff[4] used the results of a general circulation model (GCM) to examine possible runoff changes in the United States in a high-CO_2 world. Their results differed from those of Revelle and Waggoner, partly because of differences between the model-generated changes in climate and the scenario assumed in the earlier work, and partly because GCM-generated runoff data cannot be directly equated with measured riverflow (see ref. 5). Neither of these studies considered the direct effects of CO_2 on vegetation. Following Aston[6] (who used a distributed deterministic process model to simulate the effects of changed stomatal resistance on streamflow), Idso and Brazel[7] added the direct CO_2 effects associated with a CO_2 doubling to Revelle and Waggoner's analysis. The 40–70% reductions in streamflow in the absence of these direct effects became 40–60% increases when they were included. Such increases are of the same size as those predicted by Aston for catchments in eastern Australia. But how representative are these results?

If non-evaporative losses are small the mean annual water balance of a river catchment is given by

$$R = P - E \tag{1}$$

where R is runoff (here synonymous with streamflow), P is precipitation and E is evapotranspiration. The runoff ratio, γ_0, is defined by

$$R_0 = \gamma_0 P_0 \tag{2}$$

where subscript zero is used to denote present-day values. To estimate changes in runoff due to changes in precipitation and evapotranspiration we denote the change in precipitation (from P_0 to P_1) due to a doubling of atmospheric CO_2 by

$$P_1 = \alpha P_0 \tag{3}$$

Changes in evapotranspiration will occur for two reasons, as a result of climatic change and through direct CO_2-induced changes in vegetation. If we use β to denote the fractional change in evapotranspiration

$$E_1 = \beta E_0 = \beta_1 \beta_2 \beta_3 E_0 \tag{4}$$

then β can be considered conceptually as the product of three factors, β_1 the change due to a change of climate, β_2 the change due to a change in the area of vegetated cover (due to either climatic change and/or direct effects of CO_2 on plant growth), and β_3 the direct CO_2 effect on evapotranspiration. For a doubling of CO_2, β_3 is given approximately (and conservatively) by

$$\beta_3 \simeq 1 - 0.3a \tag{5}$$

where a is the fractional vegetated area of the drainage basin (see ref. 7). Manipulation of the above equations yields

$$\frac{R_1}{R_0} = \frac{\alpha - (1-\gamma_0)\beta}{\gamma_0} \tag{6}$$

This result can be used to assess the relative sensitivity of runoff changes to changes in precipitation (α) and/or changes in evapotranspiration (β). In particular, direct CO_2 effects can be studied using equation (5). The relative sensitivity is given by

$$\left| \frac{\partial(R_1/R_0)}{\partial\alpha} \Big/ \frac{\partial(R_1/R_0)}{\partial\beta} \right| = \frac{1}{1-\gamma_0}$$

Thus, runoff is always more sensitive to precipitation changes than to evapotranspiration changes, particularly for higher values of γ_0. Individual sensitivities, however, are higher for small γ_0. $\partial(R_1/R_0)/\partial\alpha$ always exceeds one, so that precipitation changes have an amplified effect on runoff, particularly in arid regions where γ_0 is small. This is a well-known result (see, for example, ref. 8). $|[\partial(R_1/R_0)]/\partial\beta|$ exceeds one for $\gamma_0 < 0.5$, so evapotranspiration changes only have an amplified effect for small γ_0.

Figure 1 shows the change in runoff for various changes in annual mean precipitation in the presence of a maximum direct

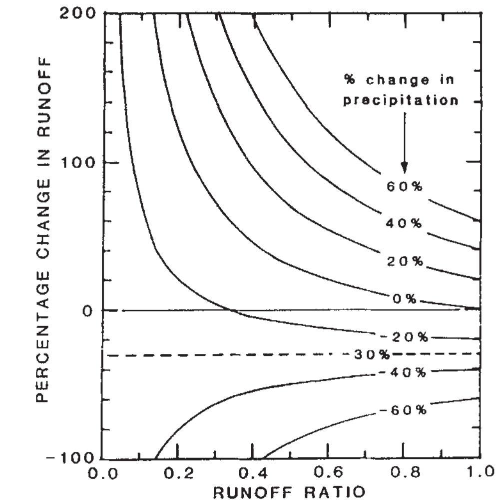

Fig. 1 Runoff changes due to changes in precipitation from a 60% reduction ($\alpha = 0.4$) to a 60% increase ($\alpha = 1.6$) assuming a maximum direct CO_2 effect on evapotranspiration ($a = 1$ in equation (5)) and no other changes in evapotranspiration ($\beta_1 = \beta_2 = 1$).

Table 1 Runoff ratios for some of the world's major rivers, listed approximately in order of mean annual discharge

River	Runoff ratio	River	Runoff ratio	River	Runoff ratio
Amazon	0.47	Parana	0.20	Niger	0.19
Congo	0.25	St Lawrence	0.33	Indus	0.40
Yangtze	0.50	Irrawaddy	0.60	Yukon	0.48
Brahmaputra	0.65	Ob	0.24	Nile	0.10
Ganges	0.42	Amur	0.32	São Francisco	0.15
Yenisey	0.42	McKenzie	0.40	Rhone	0.46
Mississippi	0.21	Columbia	0.51	Vistula	0.22
Orinoco	0.46	Zambezi	0.12	Volga	0.28
Lena	0.46	Danube	0.30	Murray	0.04

The values presented (based on ref. 15) can only be taken as a general guide. Data from different sources can vary widely because of difficulties in estimating natural flows and catchment area precipitation.

CO_2 effect ($a = 1$). For smaller runoff ratios (that is, more arid regions) any given change in precipitation has an increasingly large effect on runoff. When $\alpha = 0.7$ and $a = 1$, equation (6) reduces to $R_1 = 0.7\,R_0$, so that the runoff change is independent of the runoff ratio. For $0.7 < \alpha < 1.0$, runoff may increase or decrease depending on the value of γ_0. For $\alpha > 1.0$ runoff always increases (as the precipitation and evapotranspiration changes act in the same direction). The magnitude of the increase can be very large for small runoff ratios.

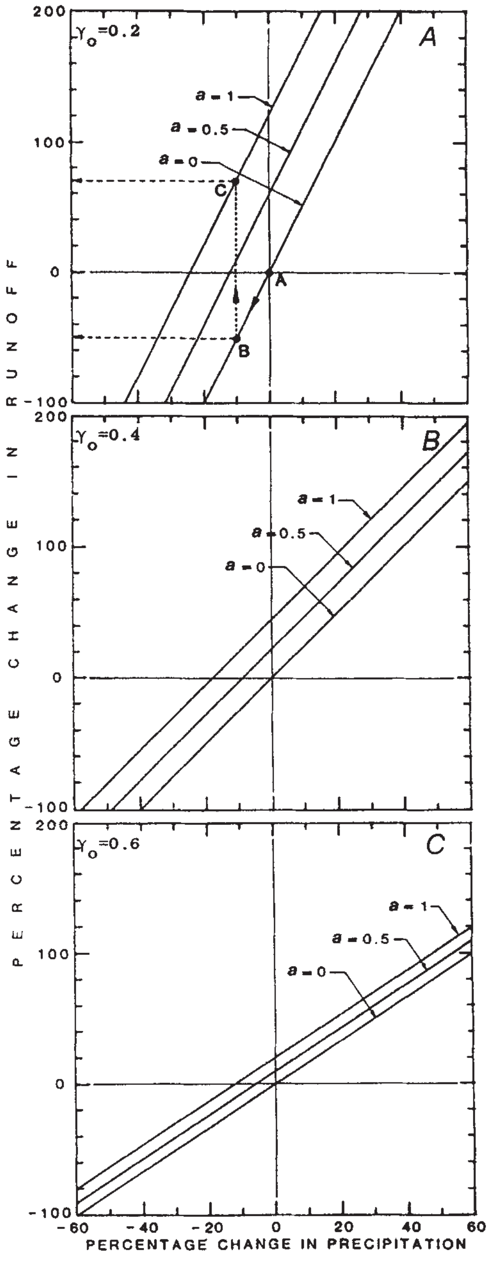

Fig. 2 Runoff changes due to precipitation changes for different evapotranspiration changes. $a = 0$ corresponds to no change in evapotranspiration, whereas $a = 1$ corresponds to a 30% reduction in evapotranspiration (the maximum direct CO_2 effect). The sensitivity to both precipitation change and evapotranspiration change increases for decreasing runoff ratio, γ_0. Three values of γ_0 are shown (A, $\gamma_0 = 0.2$; B, $\gamma_0 = 0.4$; C, $\gamma_0 = 0.6$) spanning the most common range of observed values. A ($\gamma_0 = 0.2$) includes a specific illustration. The effects of precipitation change alone are determined by the $a = 0$ lines. The line AB, therefore, shows the effect of a 10% reduction in precipitation. The effects of evapotranspiration change are determined by paths parallel to the ordinate. Thus, BC corresponds to a range of evapotranspiration reduction from 0% (point B) to 30% (point C). Point C (and the lines $a = 1$ in general) corresponds to the maximum direct CO_2 effect, but the precise cause of the evapotranspiration change is unimportant.

Table 1 lists runoff ratios for some major rivers. Values range from 0.1 or less for rivers which flow through arid regions up to more than 0.6 for some tropical rivers. In temperate latitudes, runoff ratios around 0.4 are fairly typical. Equation (6) may not be directly applicable to rivers with the lowest runoff ratios in Table 1. Some of these obtain most of their water from relatively small, high precipitation headwater catchments and then flow through arid and largely unvegetated regions. The runoff ratios given in Table 1 are for the whole drainage basin and may, in these cases, fail to represent conditions in the hydrologically-active parts of the basin.

Figure 2 shows the sensitivity of the runoff-change–precipitation-change relationship to the direct effects of CO_2 for various values of the runoff ratio. The magnitude of the direct effect can be varied by changing the parameter a. When $a = 0$ the direct effect is zero, and when $a = 1$ the direct effect is a maximum. The effects of climate related changes in evapotranspiration can also be studied using Fig. 2 since the range $a = 0$ to 1 corresponds to a range of β values from 1.0 to 0.7, that is to a range of reductions in evapotranspiration from 0 to 30%. The slopes of the lines in Fig. 2 are greatest for smallest γ_0, showing that precipitation changes have maximum effect for small γ_0. Thus, for small γ_0 (as noted earlier), precipitation changes may show a considerably amplified effect in runoff.

As an example, for a catchment with present runoff ratio of 0.2, the effect of a 10% reduction in precipitation may range from a 50% reduction in runoff with no direct CO_2 effect, to a 70% increase in runoff with a maximum direct CO_2 effect. For higher runoff ratios the range of possible runoff changes is less (see Fig. 2). In both Aston's[6] study and the Idso and Brazel[7] study, runoff ratios were low, around 0.16 in the latter case. This low value explains why Idso and Brazel obtained such vastly different results from Revelle and Waggoner[3] when they incorporated the direct effects of CO_2. Table 1 shows that such low runoff ratios are unusual. Nevertheless, the direct CO_2 effect can still be substantial for more common runoff ratios. Idso and Brazel's case may also be unrepresentative of global conditions because they assumed precipitation reductions due to increasing CO_2 (following Revelle and Waggoner[3]). Climate model results all point to an increase in the intensity of the hydrological cycle and an overall (albeit slight) increase in global mean precipitation. There will, of course, be regionally and seasonally specific exceptions to this overall trend, but, in general, the effects of precipitation change and vegetation changes can be expected to reinforce each other. In some regions, therefore, we might expect very large increases in annual mean runoff, unless these are compensated by large climate-related increases in evapotranspiration.

The extent of this compensation is difficult to estimate because the magnitudes of climate-related changes in evapotranspiration due to increasing CO_2 are unknown. Over the land, evapotranspiration changes will result from several competing factors: warmer temperatures, changes in the length of the growing (evaporative) season, changes in wind speed, changes in cloudiness, and so on. Some of these factors may cause either increases or decreases in evapotranspiration. Although existing GCMs have recognized deficiencies in the way they model the hydrological cycle[9], they still provide the best available guide to the climatic effects of increasing CO_2. All GCMs show an increase in the intensity of the global hydrological cycle. The increases vary considerably from model to model and are larger for models which show greater global-mean warming. For a doubling of CO_2 the global-mean increases in precipitation and evaporation range between about 3% (ref. 10) and 11% (ref. 4). These increases in evaporation are much less than the maximum direct CO_2 transpiration effect. However, there may be appreciable regional and/or seasonal departures from the global mean (see ref. 4) so, at least in some regions, we might expect the climate effects to modify the direct effects significantly.

The above analysis ignores several important factors. For example, the seasonal distribution of precipitation may be very different from that of evapotranspiration, and direct CO_2 effects may be diminished if the major contribution to runoff is in the winter months[11]. Seasonal effects are, however, complex. For example, if E is defined as the residual of $P-R$ (equation (1)), then our results are independent of the seasonal distribution of precipitation. Direct CO_2 effects may also be reduced if increasing CO_2 causes an increase in leaf temperatures, in individual plant leaf areas or in the total vegetated area of a catchment[11,12]. More complex catchment models (such as the statistical models of Wright[13] and Jones[14], or deterministic models like that used by Aston[6]) are required to study these effects. Our study does, however, provide a basis for first estimates of annual mean runoff changes for any river whose runoff ratio is known, and allows one to identify regions most likely to experience large runoff changes due to increasing CO_2.

Carbon dioxide research in the Climatic Research Unit is supported by the US Department of Energy under grants DE-AC02-79EV10098 and DE-AC02-81EV10738. We thank T. C. Atkinson for useful comments.

Received 21 November 1984; accepted 14 January 1985.

1. NRC *Changing Climate* (National Academy, Washington DC, 1983).
2. Lemon, E. R. (ed.) *CO_2 and Plants: The Response of Plants to Rising Levels of Atmospheric Carbon Dioxide.* A.A.A.S. Selected Symp. No. 84 (Westview, Boulder, Colorado, 1983).
3. Revelle, R. R. & Waggoner, P. E. in *Changing Climate*, 419-432 (National Academy, Washington DC, 1983).
4. Rind, D. & Lebedeff, S. *Potential Climatic Impacts of Increasing Atmospheric CO_2 with Emphasis on Water Availability and Hydrology in the United States* (United States Enviromental Protection Agency Report, 1984).
5. Nemeč, J. in *Variations in the Global Water Budget* (eds Street-Perrott, A., Beran, M. & Ratcliffe, R.) 479-488 (Reidel, Dordrecht, 1983).
6. Aston, A. R. *J. Hydrol.* **67**, 273-280 (1984).
7. Idso, S. B. & Brazel, A. J. *Nature* **312**, 51-53 (1984).
8. Schaake, J. C. Jr & Kaczmarek, Z. in *Proc. World Climate Conf.* W.M.O. No. 528, 290-312 (World Meteorological Organization, Geneva, 1979).
9. Dickinson, R. E. in *Geophys. Monogr.* No. 29, Maurice Ewing Vol. 5 (eds Hansen, J. E. & Takahashi, T.) 58-72 (American Geophysical Union, Washington DC, 1984).
10. Manabe, S. & Stouffer, R. J. *J. geophys. Res.* **85**, 5529-5554 (1980).
11. Wigley, T. M. L., Briffa, K. R. & Jones, P. D. *Nature* **312**, 102-103 (1984).
12. Morison, J. I. L. & Gifford, R. M. *Aust. J. Pl. Physiol.* **11**, 361-374 (1984).
13. Wright, C. E. *Synthesis of River Flows from Weather Data* (Tech. Note No. 26, Central Water Planning Unit, Reading, UK, 1978).
14. Jones, P. D. *J. Climatol.* **4**, 171-186 (1984).
15. Korzun, V. I. (ed.) *World Water Balance and Water Resources of the Earth* (English transl., UNESCO, Paris, 1978).

Gypsum precipitation from cold brines in an anoxic basin in the eastern Mediterranean

Scientific staff of Cruise *Bannock* 1984-12*

In 1968 hot brines from which gypsum had precipitated were discovered in the Red Sea, in a divergent plate boundary setting with hydrothermal activity[1]. We now report the discovery of cold brines in an entirely different geodynamic situation, a convergent plate boundary in the eastern Mediterranean, where the heatflow is very low[2] and no hydrothermal activity occurs. Decimetric pure gypsum crystals precipitate from the cold brines, which occupy the bottom of a rimmed anoxic basin near the southern edge of the Mediterranean Ridge, close to the Sirte Abyssal Plain. Nucleation of the crystals does not occur at the surface, but from the deep brines, because the salinity of the water is normal down to the depth of −3,000 m. We propose the name 'Bacino Bannock' for this basin, after the Consiglio Nazionale delle Ricerche R/V *Bannock* from which the bottom-water brines were surveyed and sampled.

* The following participated in the *Bannock* cruise: M. B. Cita†, K. A. Kastens‡, F. W. McCoy‡, F. Aghib†, A. Cambi§, A. Camerlenghi†, C. Corselli†, E. Erba†, M. Giambastiani†, T. Herbert‖, C. Leoni†, P. Malinverno†, A. Nosetto† & E. Parisi†.
† Department of Earth Sciences, University of Milano, Milano, Italy. ‡ Lamont-Doherty Geological Observatory of Columbia University, Palisades, New York, USA. § Department of Earth Sciences, University of Firenze, Firenze, Italy. ‖ Department of Geology, Princeton University, Princeton, New Jersey, USA.

Another anoxic basin containing highly saline bottom waters was discovered last year in the western Strabo Trench, north of the Mediterranean Ridge, and named Tyro Basin[3]. Bacino Bannock differs from Tyro in that gypsum precipitation is only recorded in the former.

Bacino Bannock was discovered using Seabeam and Seamarc I during the *Robert D. Conrad* Cruise 25-06 (April 1984). In September 1984, *Bannock* Cruise 84-12 completed a narrow-beam echosounder bathymetric survey of the basin, obtained 10 cores and two dredges, and conducted three CTD (conductivity/temperature/depth) stations and one Nansen-bottle hydrocast. Navigation on both *Conrad* and *Bannock* was by Loran-C and transit satellites.

Bacino Bannock is an irregular depression (Fig. 1) about 8 nautical miles (15 km) in diameter, within the irregular 'cobblestone topography' of the Mediterranean Ridge. A prominent bulge occupies the centre of the basin, surrounded by a moat-like depression. The Bannock sampling programme was concentrated on, and to the west of, the central bulge, where the depression is deepest.

Sediment cores (Fig. 2) from 3,000 m and shallower contain the typical eastern Mediterranean pelagic stratigraphy of sapropels and tephras. However, bottom sediments collected deeper than 3,200 m are black to dark grey and smell strongly of hydrogen sulphide. This anoxic environment contains a stratigraphy of tephra layers, breccias, carbonate sands and graded sands and silts. All samples examined at sea were richly fossiliferous, with varying proportions of planktonic and displaced benthic foraminifera (*Asterigerinata mamilla*, *A. planorbis*, *Asterigerina* sp., *Gavelinopsis lobatulus*, *Rosalina globularis*, etc.), calcareous nannoplankton and siliceous plankton. Anoxic sediments are over 9 m (implying a sedimentation rate of 10 cm kyr^{-1} in our longest core) and range in age from Holocene, probably to middle Pleistocene, as based on a combination of calcareous nannofossil biostratigraphy (*Gephyrocapsa oceanica* Zone) and planktonic foraminiferal palaeoecology.

A basal normal contact between anoxic and pre-anoxic sediments was not recovered. However, two cores (below 3,150 m, 05 and 06 GC) recovered oxic pelagic sediments of middle and late Pliocene age unconformably beneath Holocene anoxic sediments and in a breccia, respectively.

Abundant gypsum in cores and dredge hauls was the most surprising discovery at Bacino Bannock. In cores, individual crystals range in size from microscopic to the full diameter of the core barrel (7 cm). The dredges recovered enormous masses of interlocked gypsum crystals, up to 0.5 m across (Fig. 3). Both dredges were caught up in the gypsum and required more than 5 tons of pull and several hours (more than 24 h at station 11 D) to be freed. These composite gypsum masses were only recovered from the steep western wall of the central bulge where they adhered to a hard substrate of grey Pleistocene marlstone. individual crystals in cores and dredges were both tabular and bipyramidal and many contained inclusions concentrated along crystal planes. Inclusions consisted of pelagic debris such as planktonic foraminifera (Fig. 4), including *Globigerina bulloides*, *Globigerinoides ruber* and *Orbulina universa*, pteropods, including the Holocene species *Cavolinia gibbosa*, and *Cavolinia inflexa*, *Clio pyramidata* and *Atlanta* sp., and mineral grains.

Rubbery mats, similar to those described from the Tyro Basin[3] and consisting of organic fibres containing diatoms, planktonic foraminifera and mineral grains, were found in both cores and dredges. In cores, the mats were recovered as horizontal disks, presumably cut from larger mats as though by a biscuit cutter; in dredges they occurred between crystals, with no preferred orientation.

CTD measurements indicate normal Mediterranean deep-water down to 3,000 m (the length of the conducting hydro-cable on board). A 15-kHz echosounder recorded horizontal reflectors within the water column at depth of 3,228, 3,428 and 3,325 m, suggesting locally-high gradients in temperature, salinity and/or particulate matter. During coring and hydrocast operations, the depth of the instrument was monitored by an acoustic pinger